Polycrystalline $ZrTe_5$ Parametrized as a Narrow-Band-Gap Semiconductor for Thermoelectric Performance

Samuel A. Miller,[1] Ian Witting,[1] Umut Aydemir,[1,2] Lintao Peng,[3] Alexander J. E. Rettie,[4] Prashun Gorai,[5,6] Duck Young Chung,[4] Mercouri G. Kanatzidis,[4,7] Matthew Grayson,[3,8] Vladan Stevanović,[5,6] Eric S. Toberer,[5,9] and G. Jeffrey Snyder[1,*]

[1]*Department of Materials Science and Engineering, Northwestern University, Evanston, Illinois 60208, USA*
[2]*Department of Chemistry, Koç University, Sariyer, Istanbul 34450, Turkey*
[3]*Applied Physics Graduate Program, Northwestern University, Evanston, Illinois 60208, USA*
[4]*Materials Science Division, Argonne National Laboratory, Argonne, Illinois 60439, USA*
[5]*National Renewable Energy Laboratory, Golden, Colorado 80401, USA*
[6]*Department of Metallurgical and Materials Engineering, Colorado School of Mines, Golden, Colorado 80401 USA*
[7]*Department of Chemistry, Northwestern University, Evanston, Illinois 60208, USA*
[8]*Department of Electrical Engineering and Computer Science, Northwestern University, Evanston, Illinois 60208, USA*
[9]*Department of Physics, Colorado School of Mines, Golden, Colorado 80401 USA*

(Received 25 August 2017; revised manuscript received 22 November 2017; published 24 January 2018)

The transition-metal pentatellurides $HfTe_5$ and $ZrTe_5$ have been studied for their exotic transport properties with much debate over the transport mechanism, band gap, and cause of the resistivity behavior, including a large low-temperature resistivity peak. Single crystals grown by the chemical-vapor-transport method have shown an n-p transition of the Seebeck coefficient at the same temperature as a peak in the resistivity. We show that behavior similar to that of single crystals can be observed in iodine-doped polycrystalline samples but that undoped polycrystalline samples exhibit drastically different properties: they are p type over the entire temperature range. Additionally, the thermal conductivity for polycrystalline samples is much lower, 1.5 Wm^{-1} K^{-1}, than previously reported for single crystals. It is found that the polycrystalline $ZrTe_5$ system can be modeled as a simple semiconductor with conduction and valence bands both contributing to transport, separated by a band gap of 20 meV. This model demonstrates to first order that a simple two-band model can explain the transition from n- to p-type behavior and the cause of the anomalous resistivity peak. Combined with the experimental data, the two-band model shows that carrier concentration variation is responsible for differences in behavior between samples. Using the two-band model, the thermoelectric performance at different doping levels is predicted, finding $zT = 0.2$ and 0.1 for p and n type, respectively, at 300 K, and $zT = 0.23$ and 0.32 for p and n type at 600 K. Given the reasonably high zT that is comparable in magnitude for both n and p type, a thermoelectric device with a single compound used for both legs is feasible.

DOI: 10.1103/PhysRevApplied.9.014025

I. INTRODUCTION

Thermoelectric (TE) materials are those that convert a temperature gradient to a voltage or an electrical current flow into a heat flow, with applications in power generation and Peltier cooling. This thermoelectric conversion of heat energy into electrical energy, the Seebeck effect, has been well studied, with compounds optimized for use in various temperature ranges and applications. Mid- and high-temperature thermoelectrics have been well investigated, including PbTe, SiGe, and Zintl compounds [1–5]. However, there is a dearth of materials for applications at lower temperatures. To date, TE materials for cooling applications fall into one of three families: $Bi_{1-x}Sb_x$ [6,7], $CsBi_4Te_6$ [8,9], or $(Bi,Sb)_2(Te,Se)_3$ [10,11]. Furthermore, construction of thermoelectric generators requires thermal and chemical stability and matching between the n and p legs of the device [12]. Recently, there has been interest in the use of layered transition-metal pentatellurides for low-temperature thermoelectric applications. $ZrTe_5$ and $HfTe_5$ have demonstrated high power factors, though the thermal conductivity is relatively high [13,14]. Measurement of needlelike single

*Corresponding author.
jeff.snyder@northwestern.edu

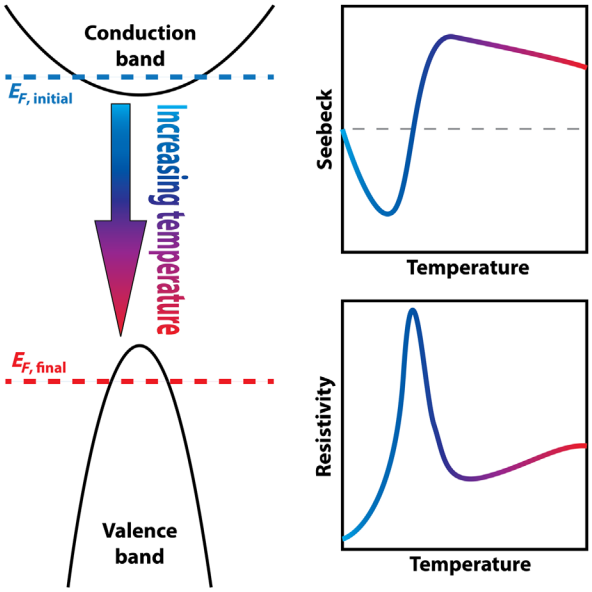

FIG. 1. Schematic of the two-band model for the iodine-doped polycrystalline sample (or vapor-grown single crystals) showing movement of the Fermi level with increasing temperature and the resulting properties.

crystals showed the thermal conductivity to be in the range of approximately 4–8 Wm^{-1} K^{-1} at room temperature [15]. In contrast, recent calculations indicated that the lattice thermal conductivity should be much lower [16–18], and, thus, the zT higher than initially thought, warranting further study [19].

However, the optimization of thermoelectric performance through compositional tuning of the pentatelluride materials has been difficult due to a poor understanding of the underlying transport. Chemical-vapor-grown single crystals of $ZrTe_5$ exhibit a peak in resistivity (ρ) as a function of the temperature and a change in sign of the Seebeck coefficient (α) at approximately 130 K. There have been many explanations for this behavior over the years. Researchers first believed this was due to charge-density waves [20], but diffraction, magnetic field, and compositional data indicated this was not likely the cause of the peaked resistivity [21,22]. Other explanations have since been advanced, but there has not been consensus on the cause of the transport phenomena [23,24]. The temperature-induced Lifshitz transition has been studied as well as the quantum Hall effect and chiral magnetic effect [25–30], but there remains a debate over whether pentatellurides are topological insulators with a small band gap or whether they are Dirac semimetals [31–36].

To more specifically investigate the promise of $ZrTe_5$ as a thermoelectric material, we produce bulk polycrystalline $ZrTe_5$ samples. Our undoped samples are p type over the entire temperature range, though substitution of iodine for tellurium causes a transition to n type at low temperatures, in agreement with previous reports. Using the experimental Seebeck coefficient, thermal conductivity (κ), and Hall data, we find that in the polycrystalline form, these pentatellurides can be modeled as a narrow-band-gap semiconductor with effective contributions from a single n-type conduction band and a single p-type valence band. We then use our model to explain previous property observations in the literature and are able to explain the resistivity peak in terms of an n-type to p-type thermally induced crossover shown schematically in Fig 1. We also investigate predicted thermoelectric properties from this model and show how to optimize the zT for these polycrystalline materials, as well as note their potential use for both n- and p-type legs in the same device.

II. METHODS

Bulk polycrystalline $ZrTe_{5-x}I_x$ samples are produced by solid-state reaction of Zr (Alfa Aesar, 99.95%), Te (Alfa Aesar, 99.999%), and TeI_4 (Strem Chemical, 99.9%) followed by hot pressing. Zr is mixed in a stoichiometric ratio with Te and TeI_4, placed in a quartz ampule, evacuated to 10^{-5} mbar, and torch sealed. Using a vertical single-zone furnace, the heating profile is 90 K/h from room temperature to 923 K, dwell time of 12 h, furnace quench (300 K/h) to 748 K, dwell for 72 h, and finally cooling to room temperature at 90 K/h. The resulting material is ground in an agate mortar and pestle into a fine powder. The powder is hot pressed in a half-inch graphite die using a maximum temperature of 723 K for 2 h under flowing argon followed by ambient cooling. A series of grit papers ending in 1200 grit is used to polish residual graphite foils and produce samples of uniform thickness.

X-ray diffraction is used to monitor the sample purity by a Rigaku D/Max diffractometer. A Netzsch LFA 457 is used to measure the thermal diffusivity at high temperatures, and the Dulong-Petit approximation is applied for the heat capacity. The Hall coefficient and ρ are measured using a four-point van der Pauw technique with a 2-T magnet under high vacuum, while a light-pipe method utilizing chromel-niobium thermocouples is used to measure the Seebeck coefficient [37,38]. For the low-temperature measurements, a number of instruments are used to measure the various properties. A Physical Property Measurement System (PPMS, Quantum Design) is used in the van der Pauw configuration as well as with the Thermal Transport Option (TTO). For all PPMS measurements, the contacts are made out of silver paste, air dried, and are Ohmic in the temperature range considered. Additional low-temperature magnetotransport and Hall measurements are done on square planar devices with four-corner contacts applying the van der Pauw method. The experiment is conducted in a Cryogenic Ltd. cryogen-free 5-T magnet system with a helium flow cryostat using ac lock-in techniques (SR830).

To model and analyze the thermoelectric transport data, the effective mass model is used [39]. This model is frequently employed to guide the understanding and

optimization of thermoelectrics. However, there are cases where the effective mass model breaks down, namely, due to nonparabolic bands or multiband effects [40–42]. We consider two bands contributing to transport and restrict the use of the model to higher temperatures where any possible topological and phase-coherent effects are suppressed. One valence and one conduction band are used, both with a rigid band shape that does not change with the temperature or doping level. In this model, the effective mass and initial doping level for each band are fixed along with the band gap. To calculate the Fermi level at each temperature, the charge neutrality condition is used for the chemical potential relationship between two bands with known gap. The charge neutrality is given by

$$N_d^+ + p = n + N_a^-, \tag{1}$$

where N_d^+ and N_a^- are the number of ionized donors and acceptors, respectively, and p and n are the concentrations of holes and electrons. For a given band gap E_g, the relationship between the reduced chemical potentials of the two bands is given by the expression

$$\eta_1 = -\eta_2 - \frac{E_g}{k_B T}. \tag{2}$$

Once the masses, dopant level, and band gap are set and the Fermi level at each temperature is calculated, the properties of each band according to the effective mass model can be determined. These properties are given below for a two-band system, though they can be generalized to multiband with the appropriate summations:

$$\alpha_{\text{tot}} = \frac{\alpha_1\sigma_1 + \alpha_2\sigma_2}{\sigma_1 + \sigma_2}, \tag{3}$$

$$\sigma_{\text{tot}} = \sigma_1 + \sigma_2, \tag{4}$$

$$R_{H,\text{tot}} = \frac{R_{H,1}\sigma_1^2 + R_{H,2}\sigma_2^2}{\sigma_{\text{tot}}^2}, \tag{5}$$

where α, σ, and R_H are the Seebeck coefficient, electrical conductivity, and Hall coefficient, respectively. The subscripts 1 and 2 denote the contribution from each of the two bands (in this case, one conduction and one valence, though this analysis can be applied to two bands of the same type). The total thermal conductivity (κ_{tot}) is then given by

$$\kappa_{\text{tot}} = \kappa_L + T(L_1\sigma_1 + L_2\sigma_2) + T\left((\sigma_1\alpha_1^2 + \sigma_2\alpha_2^2) - \frac{(\sigma_1\alpha_1 + \sigma_2\alpha_2)^2}{\sigma_1 + \sigma_2}\right). \tag{6}$$

Here, the first term, the lattice thermal conductivity (κ_L), is set in the model to have some temperature dependence. At high temperature, Umklapp scattering dominates, which has a T^{-1} dependence. The second term is the electronic thermal conductivity, which depends on the temperature, electrical conductivity, and Lorentz number (L). The third term is bipolar thermal conductivity.

III. RESULTS AND DISCUSSION

A. Synthesis and characterization

Most previous reports of $ZrTe_5$ properties have been for single crystals grown by a chemical-vapor-transport method. For these crystals, the Seebeck coefficient is linear at low temperature, changes from n to p type near 130 K, and has an absolute value of approximately 100–200 μV K^{-1}, while the temperature-dependent resistivity has a peak around 130 K, which is a few times higher than the room-temperature value [13,14,43–49]. Recently, a tellurium self-flux-growth technique was used to synthesize single crystals, an alternative to the traditional vapor-transport growth [25]. These flux-grown crystals exhibit similar behavior as chemical-vapor-transport single crystals in general, though there are some key differences when compared with vapor-grown crystals. For example, ρ does not trend toward zero at 0 K, the n-type α is significantly larger in magnitude, and most important, the temperature is much lower for the n-p transition and resistivity peak, around 60 K. These differences indicate that synthesis techniques are very important in determining the properties of $ZrTe_5$. In addition to the influence on differences in the TE properties, both the vapor-growth and self-flux techniques produce needlelike single crystals which are small and can present challenges for property measurement and sample loading. Finally, there are seldom reports of the thermoelectric properties above 300 K [13], which would provide a more complete understanding of the transport. To resolve these issues, we synthesize the $ZrTe_5$ samples by solid-state reaction and hot pressing, producing large, bulk, polycrystalline samples for study across the entire temperature range, approximately 0 to 700 K.

$ZrTe_{5-x}I_x$ samples are prepared by solid-state reaction and hot pressing with powder XRD used to monitor the sample purity at room temperature (see Fig. S1 in the Supplemental Material [50]). Rietveld refinement is performed by the WinCSD program package [51] on the hot pressed undoped sample [52], and the result is shown in Fig. S2. All compositions labeled in the text and figures are the nominal composition. Additional details on x-ray diffraction, Rietveld refinement, and raw transport data can be found in the Supplemental Material [50]. The samples are nearly phase pure after solid-state reaction as well as following hot pressing. The geometric density of the hot-pressed samples is greater than 98% of the theoretical density for $ZrTe_5$. The Seebeck coefficient and resistivity for the polycrystalline $ZrTe_{5-x}I_x$ samples are shown in Fig. 2. While the $ZrTe_{4.85}I_{0.15}$ sample exhibits properties largely similar to previous reports on chemical-vapor-grown single-crystal samples, the behavior of

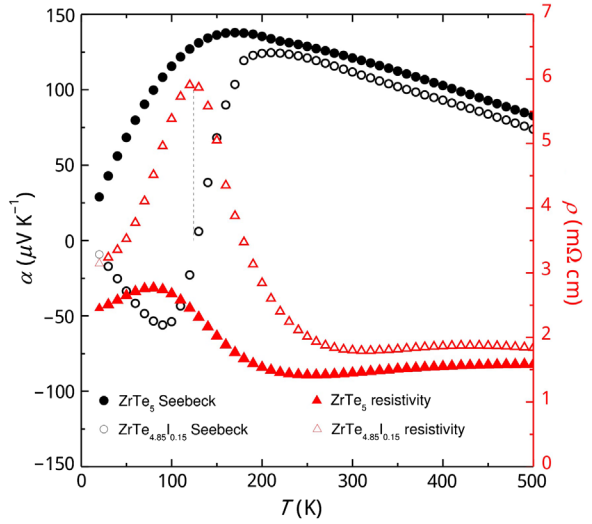

FIG. 2. Seebeck coefficient and resistivity for polycrystalline $ZrTe_5$ and $ZrTe_{4.85}I_{0.15}$. Dashed line at 130 K indicating resistivity peak and Seebeck coefficient crossing zero for $ZrTe_{4.85}I_{0.15}$. Undoped $ZrTe_5$, by contrast, has a lower temperature resistivity peak and stays p type over the full temperature range.

undoped polycrystalline $ZrTe_5$ is quite different (Fig. 2). The Seebeck coefficient for the latter is always positive, and the resistivity peak is shifted to a lower temperature, closer to 60 K, in addition to being smaller in magnitude relative to $\rho_{300\ \mathrm{K}}$.

The resistivity (ρ_{xx}) and Hall resistance (R_{xy}) as a function of magnetic field are shown in Fig. 3 for these polycrystalline samples. At low temperatures, $\rho_{xx}(B)$ shows an antilocalization minimum at $B = 0$ typically associated with strong spin-orbit coupling typical to the valence band and also the conduction band for narrow-gap materials [53]. This behavior could also be attributed to topological surface states, possibly at grain-boundary interfaces. Numerous unconventional effects have previously been observed in single crystals at low temperatures, including the chiral magnetic effect [28,29], Lifshitz transition [25,54], van Hove singularity [55,56], Zeeman splitting [57,58], and topological effects [31,33,34,53,54,59]. This measurement demonstrates that some of the unconventional effects previously observed at low temperatures in single crystals persist in polycrystalline samples as well. However, at higher temperatures, these effects are less important in their contributions to the transport behavior. As the temperature increases, $\rho_{xx}(B)$ in Fig. 3(a) is less dependent on magnetic field over the relevant magnetic field range, deviating at most ±25% around the mean value, with a sharp curvature only at the lowest temperature. Thus, we define an arbitrary cutoff of 150 K, above which we argue that a Drude-like model with no consideration of phase-coherent effects can approximate the observed behavior but below which a more careful model including weak antilocalization is needed. The Hall resistance for $ZrTe_{4.85}I_{0.15}$ is consistent with previous measurements [25]

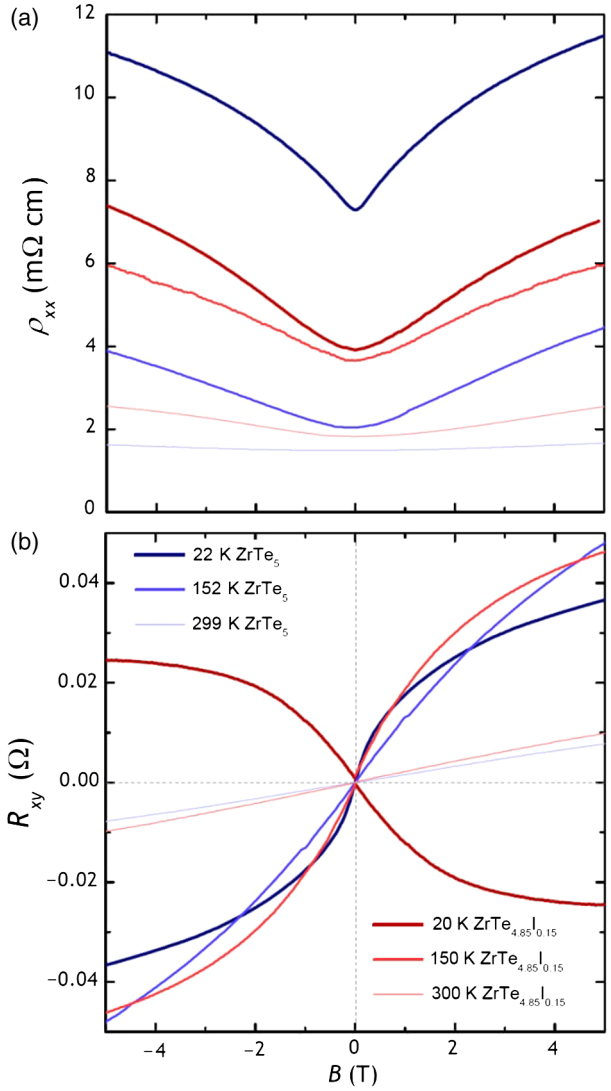

FIG. 3. Resistivity (a) and Hall resistance (b) for both $ZrTe_5$ and $ZrTe_{4.85}I_{0.15}$ at select temperatures (well below, near, and well above the transition).

and with Seebeck coefficient measurements showing n-type conduction at low temperatures and switching to p type at higher temperatures, while undoped $ZrTe_5$ remains p type at all temperatures, again consistent with Seebeck coefficient measurements. Both of the polycrystalline samples show nonlinearity of R_{xy} with B at lower temperatures, possibly indicating more than one carrier contributes to conduction. As the temperature increases, R_{xy} becomes linear with B, indicating a single charge carrier dominates.

B. Two-band modeling

Although there are prominent features in the low-temperature magnetotransport associated with spin-orbit coupling and phase-coherent scattering, as we shall demonstrate, the higher-temperature properties above 150 K can be reproduced with a simple two-band model for all of

the transport coefficients in this high temperature range. In addition, the qualitative trends at low temperature can also be reproduced with the same parametrization. We, therefore, propose a simplified two-band model that clarifies the significantly different properties observed in the $ZrTe_5$ samples produced by different methods (polycrystalline, flux, or vapor grown) and offers insight into the phenomena of the resistivity peak and Seebeck coefficient switching from n to p type. Using this simple two-band model with one valence and one conduction band, we can describe the thermoelectric properties observed for various samples by changing only the doping level.

The effective mass model used here is similar to the single parabolic band model commonly used in thermoelectrics, but it considers contributions from two bands (one conduction and one valence). To construct the model, we fix a number of parameters based on previous experimental and computational studies and then determine the mobility needed to explain the experimentally measured transport properties. The Boltzmann transport equations have previously been derived assuming the Drude model for mobility and an energy-dependent scattering time $\tau = \tau_0 E^{\lambda-1/2}$ ($\lambda = 0$ for the acoustic phonon) [60]. For the fits to the polycrystalline $ZrTe_{5-x}I_x$ samples, we fix the isotropic electron and hole Seebeck mass as $m_e = 0.5\ m_0$ and $m_h = 0.15\ m_0$, respectively, and the band gap as $E_g = 0.02$ eV. The number of donors for the iodine-doped sample is fixed at $N_d = 1.1 \times 10^{18}$ cm^{-3}, while for the undoped $ZrTe_5$ sample, the number of acceptors is $N_a = 4.5 \times 10^{17}$ cm^{-3}. To appropriately fit the data, we find that the masses, their ratio, and the band gap are required to be within a relatively narrow range. For example, it is only possible to fit the model to experimental data when the band gap is set between approximately 0.015 and 0.03 eV. Previous experimental studies using a variety of techniques have found that the band gap of $ZrTe_5$ can be anywhere from 100 meV to a gapless semimetal [27,28,31–35,54,61]. However, recent ARPES studies observed a 40-meV band gap at 255 K which decreases with decreasing temperature [54], while another measured a gap of 18–29 meV [62]. We find that the model works best with a gap of 20 meV. As this is an effective mass model, we cannot definitively determine each of the parameters without more experimental data; we can suggest only general ranges and ratios of the parameters. Additionally, an isotropic model is used here, whereas the transport properties in $ZrTe_5$ are anisotropic [58,63,64]. The transport properties are expected to be anisotropic due to the structure of $ZrTe_5$ and needlelike growth of single crystals. However, the solid-state reaction, grinding, and hot-pressing procedure used here produces a sample that is not textured, as seen in the Rietveld refinement. Instead, the sample is a collection of randomly oriented grains such that the properties for each direction are averaged out, allowing the use of a simpler, isotropic model here.

The experimental properties for both polycrystalline samples, as well as the model using two different doping levels, are shown in Fig. 4. The model fits the data reasonably well in the range of 200–600 K. The resistivity as a function of the temperature is well described by this effective mass model across the entire temperature range [Fig. 4(a)]. The Seebeck coefficient data fits well at high temperature [Fig. 4(b)]. The model deviates from the experimental data at low temperatures, though this is to be expected. As discussed previously, the unconventional transport effects start to dominate in these polycrystalline samples at low temperature. The modeled Hall coefficient qualitatively reproduces the trends observed in the experimental Hall coefficient [Fig. 4(c)], which is determined using a linear fit to the low-field R_{xy} vs B data.

The resistivity and Seebeck coefficient behavior for the $ZrTe_{4.85}I_{0.15}$ sample is very similar to previous reports for chemical-vapor-grown single crystals, showing n-type behavior at low temperature. The Seebeck coefficient is n type at low temperature and increasing in magnitude as the Fermi level is initially in the conduction band and moving toward the gap with increasing temperature. The temperature where the Seebeck coefficient crosses zero and the resistivity is at a maximum (approximately 130 K in this case) is where the Fermi level nears the middle of the gap. With increasing temperature, the Fermi level continues toward the valence band as the material becomes more p type. Finally, after the Seebeck coefficient reaches its maximum p-type value, it then decreases linearly with the temperature, when the Fermi level becomes effectively pinned within the valence band (see Fig. 1). As we demonstrate later, the initial position of the Fermi level in the conduction band is what controls the temperature at which $\alpha = 0$ and the resistivity is peaked. On the other hand, for the undoped polycrystalline $ZrTe_5$, the Seebeck coefficient is always positive due to the Fermi level residing in the valence band. At low temperatures, the Fermi level moves toward the gap leading to the linear increase in α, and eventually, it is pinned within the valence band.

The model for κ [Fig. 4(d)] considers Umklapp scattering as well as the electronic and bipolar contributions to total thermal conductivity. Umklapp scattering dominates at higher temperatures and has a T^{-1} dependence which fits the data well at higher temperatures in the area of interest for zT predictions. Below 200 K, the model fit to the experimental data is not as good, partly due to the use of a PPMS for low-temperature measurements which uses a direct measurement technique that is uncorrected for radiation. The fit below 200 K is not expected to be exact, as the measurement technique differs, and other scattering mechanisms (i.e., point defect or boundary scattering) may play a role at lower temperatures. Because of the layered crystal structure, κ is fairly low. Though $ZrTe_5$ is predicted to have a lattice thermal conductivity of 1.8 Wm^{-1} K^{-1} at 300 K [19], the initial reports in single-crystal $ZrTe_5$ found

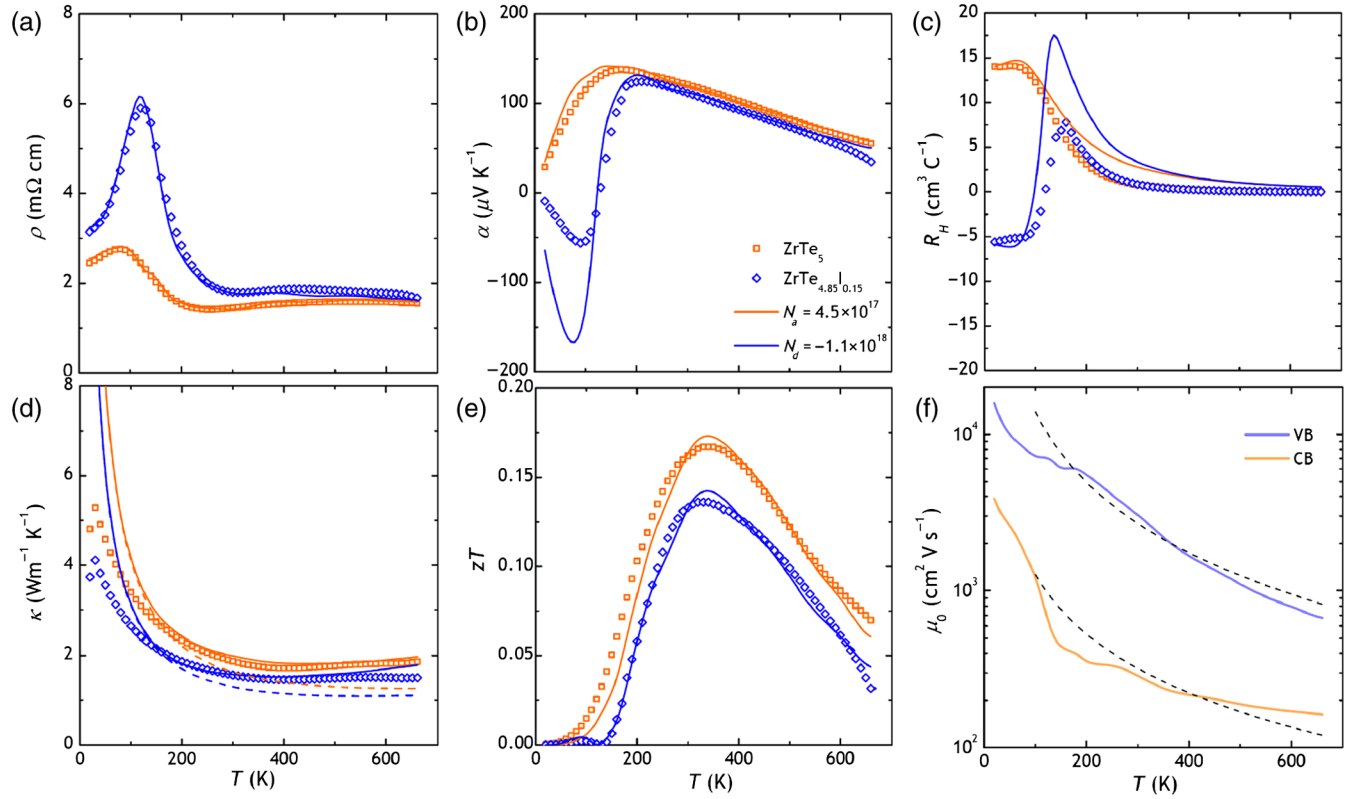

FIG. 4. Smoothed experimental data (symbols) for (a) resistivity, (b) Seebeck coefficient, (c) Hall coefficient, (d) total thermal conductivity, and (e) zT. Also shown are the modeled properties (lines) with two different carrier concentrations using the parameters listed in the text. In (e), the total (solid) and lattice plus bipolar (dashed) thermal conductivity using the model are shown. The modeled mobility is shown in (f) with dashed lines representing $T^{-3/2}$.

$\kappa \sim 8\ \mathrm{Wm^{-1}\,K^{-1}}$. However, due to the small size and needlelike shape of the single crystals measured previously, there may be a significant error in the initial report of thermal conductivity. These measurements demonstrate a much lower total thermal conductivity, experimentally confirming the prediction [Fig. 4(d)] in line with previous measurements [65]. This difference in the thermal conductivity is expected due to the polycrystalline nature, but it is also partly due to the measurement technique allowed by the larger size and shape of these samples. Our polycrystalline $ZrTe_5$ samples exhibit a total thermal conductivity 4 times lower than that measured for single crystals along the a axis, so while the power factor is reduced, the overall zT [Fig. 4(e)] is higher.

In most thermoelectric materials, it is sufficient to assume solely acoustic phonon scattering for modeling purposes, as they tend to be investigated at temperatures above 300 K. However, for these pentatelluride systems, the thermoelectric behaviors of interest occur below 200 K, where other scattering mechanisms can play a significant role. For example, in Si and Ge, ionized impurity scattering dominates the temperature dependence of mobility at low temperatures, while acoustic phonon scattering is more important at higher temperatures [60]. The Fermi integrals used in this model are for $\lambda = 0$ acoustic phonon scattering, since we are primarily concerned with high-temperature properties while the model is not expected to fit precisely at low temperatures due to the reasons discussed previously. The mobility used to fit the measured properties is shown in Fig. 4(f). The modeled mobility for both the conduction and valence bands has a temperature dependence close to $T^{-3/2}$ above 100 K, in agreement with acoustic phonon scattering.

In addition to the low-temperature effects discussed previously, there is another contribution to the discrepancy between the measured and modeled Seebeck and Hall coefficients. Because of the complex nature of the pentatellurides with a small band gap and layered structure, density-functional-theory calculations of the band structure have not always been in agreement [31,34,61,66]. Additionally, the calculated band structure is sensitive to the parameters used, including the temperature, stress or strain induced by chemical substitution, and pressure [27,58,59]. However, calculations typically show a single hole pocket centered around Γ with much higher energy than other pockets, while the conduction band has numerous pockets at comparable energy levels. As T increases, these pockets contribute to conduction leading to an increase in the Seebeck effective mass. This increase in mass is due to carriers being thermally generated across the

small gap due to broadening of the Fermi-Dirac distribution with the increasing temperature. A better fit to the experimental data can be achieved by either adding a third band or employing a temperature-dependent effective mass or band gap, but because exact fits are not expected due to the unconventional effects at low temperatures as previously discussed, the introduction of additional fitting parameters is not warranted. Nonetheless, this model does qualitatively reproduce the trends as a function of the temperature for the various property measurements.

C. Effect of varying carrier concentration

The two-band model fit to the experimental data can be extended to simulate properties at carrier concentrations not used for modeling, as shown in Fig. 5. This is done by adjusting the initial doping level in the calculations akin to experimental carrier concentration tuning using external dopants. As the p-type carrier concentration is increased, the peak in the Seebeck coefficient moves to a higher temperature and lower magnitude, while the resistivity peak decreases in magnitude. As the n-type carrier concentration is increased, the n-type Seebeck coefficient crosses 0 at a higher temperature for higher doping levels, while the resistivity peaks at a lower magnitude but a higher temperature. This qualitative behavior is in good agreement with previous measurements of single crystals with different carrier concentrations. Reports of iodine-vapor-grown crystals show n_H of approximately 1×10^{18} cm^{-3} at room temperature and an n-p transition temperature of about 130 K, while self-flux-grown single crystals had values of 5×10^{16} cm^{-3} and 60 K [13,24,25]. The trends from the two-band model in the Seebeck coefficient and resistivity are also in agreement with experiments where rare-earth elements are substituted for the transition metal (see Fig. S5 in the Supplemental Material [50] and Ref. [67]). The model predicts that at high n-type carrier concentrations, a negative Seebeck will persist to higher temperatures, as has been experimentally found for $Hf_{0.99}Ta_{0.01}Te_5$ up to at least 300 K [68].

As was previously discussed, the synthesis route used to produce the $ZrTe_5$ samples has a dramatic effect on the observed properties. Our model shows that the cause of the various properties found in different crystals is the carrier concentration variation due to processing. The traditional route for making single crystals of $ZrTe_5$, chemical-vapor-transport synthesis, is thought to produce pure samples. Iodine is used as the vapor-transport agent, so even though the crystals are washed after this procedure, it is unlikely that all iodine is removed. Substitution of I for Te will act as an electron donor causing n-type transport at low temperatures before the higher-mobility p-type conduction dominates as the carriers are thermally activated. Our model demonstrates how variations in the carrier concentration, in this case, due to unintentional doping with iodine, change the properties. This is experimentally verified by

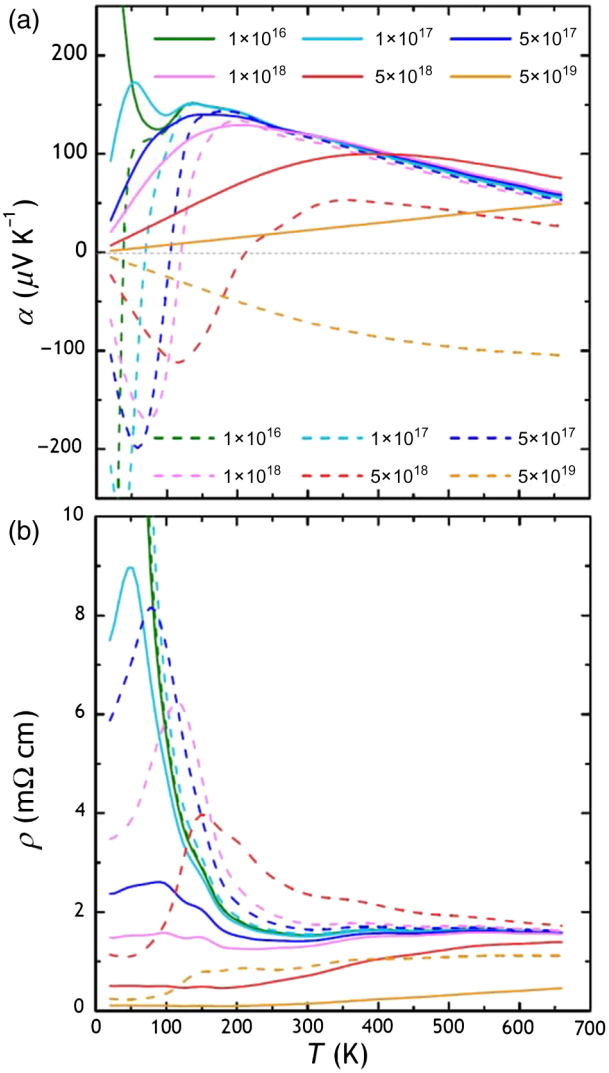

FIG. 5. The (a) Seebeck coefficient and (b) resistivity as a function of the temperature in polycrystalline $ZrTe_5$ for different doping levels (cm^{-3}) of both p (solid) and n-type (dashed) carriers.

measurements on undoped and iodine-doped polycrystalline samples. Additionally, the differences between Te self-flux-grown single crystals and undoped polycrystalline samples can be explained in the context of this model. $ZrTe_5$ is considered a line compound, though there is actually a finite phase width. So, while both the flux and solid-state reactions consist of only Zr and Te (no I), the ratio of the two elements may vary in the samples produced by different methods. This Zr:Te ratio will lead to changes in carrier concentration due to differences in actual (not nominal) stoichiometry. For example, Te vacancies caused by the high vapor pressure of tellurium will act as electron donors. Our model shows that the temperature and magnitude of the ρ peak as well as the n-p transition of α can be tuned by adjusting the carrier concentration accomplished through careful control of the Zr:Te ratio or dopant concentration.

D. Tuning model to optimize thermoelectric performance

Because of the reasons previously stated, we do not expect the model to be accurate at low temperatures, but the properties are well fit in the range of 200–600 K, where the peak zT is observed. Figure 6(a) shows the zT as a function of the temperature for various doping levels, while Fig. 6(b) shows the zT vs doping level for both p- and n-type samples at various temperatures. With low doping levels, bipolar conduction sets in by 200 K, leading to modest zT. However, as the doping level is increased, the maximum zT increases as the Fermi level is pinned into one band or the other. Controlling the carrier concentration allows for optimization of the zT in a desired temperature range.

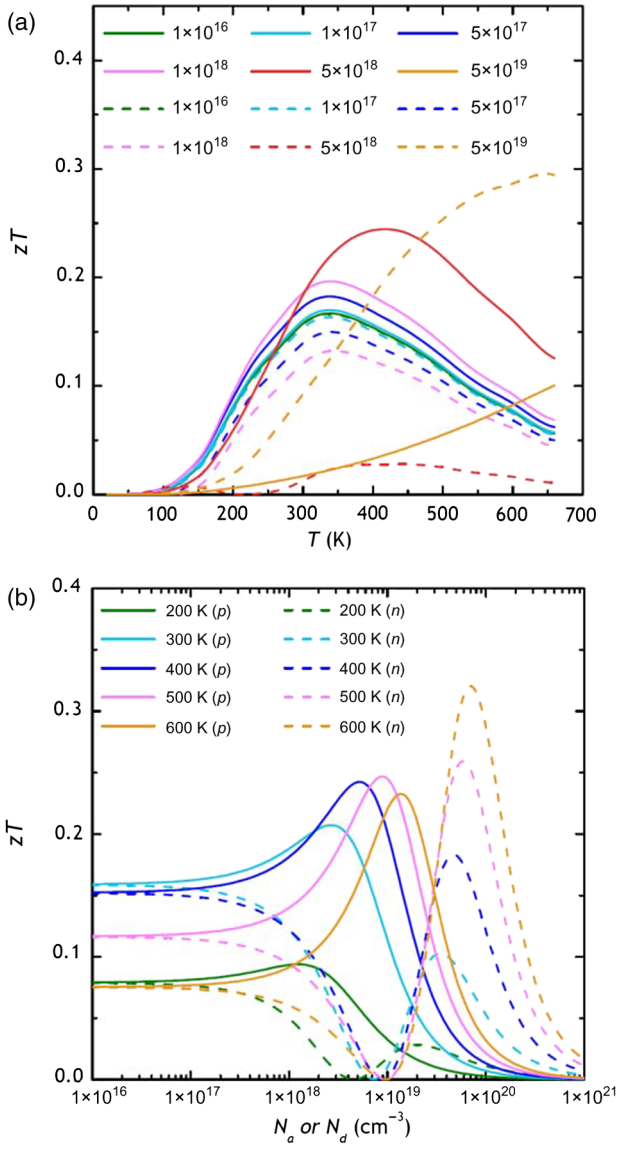

FIG. 6. For polycrystalline $ZrTe_5$, (a) the zT as a function of temperature at various acceptor (solid) or donor (dashed) levels, and (b) the zT as a function of dopant concentration for temperatures ranging from 200 to 600 K.

Using the model for predictions, strategies can be devised for optimizing the thermoelectric performance of $ZrTe_5$. By increasing the band gap, minority-carrier contributions can be suppressed, increasing the zT to approximately 0.4 at 300 K. Increasing the band gap can be achieved by substitution of Se for Te, as demonstrated previously [68]. Using our two-band model, we can estimate the zT contributions of each band independently. From this, we observe that engineering the composition such that the mobility of the minority carrier is reduced by a factor of 10 will also increase the zT at 300 K to approximately 0.35 for p type. A two- to threefold reduction in the lattice thermal conductivity through grain size reduction, softening of the lattice, alloying, or other strategies will potentially lead to a zT near 1 at room temperature. Furthermore, by controlling the carrier concentration through doping, n and p legs can be made in the $ZrTe_5$ system, providing the opportunity to make modules out of a single compound, thus, mitigating issues with chemical and thermal compatibility.

IV. CONCLUSIONS

The details of transport in the $HfTe_5$ and $ZrTe_5$ systems have been debated for many years due to the exotic transport properties observed in single crystals. The measurement of polycrystalline $ZrTe_5$ samples reveals p-type behavior at all temperatures, leading to a conjecture that the system can be explained as a semiconductor. Doping $ZrTe_5$ with iodine leads to properties similar to previous reports on single crystals, with an n to p transition near 130 K, suggesting that prior work on pentatellurides may have been contaminated by residual iodine from the typical iodine-vapor-transport synthesis. A two-band model is constructed which accurately describes the properties of polycrystalline samples as well as explains the behavior of both flux- and vapor-grown single crystals. The model has a temperature-independent band gap of 0.02 eV, a valence band with a higher mobility, and a conduction band with a higher effective mass. The experimental data are consistent with a semiconductor having a positive finite gap where the anomalous resistivity peak and change in Seebeck coefficient can be simultaneously explained. Finally, the model allows for prediction of zT by carrier concentration tuning and other strategies to optimize the thermoelectric performance. $ZrTe_5$ is promising for practical applications, as a thermoelectric device can be constructed out of a single material used for both legs.

ACKNOWLEDGMENTS

The authors thank Thomas O. Mason for helpful discussions. We acknowledge primary support from the National Science Foundation Division of Materials Research (DMR) program, Grants No. 1334713, No. 1334351, and No. 1333335. The research is performed using computational resources sponsored by the

Department of Energy's Office of Energy Efficiency and Renewable Energy and located at the National Renewable Energy Laboratory (NREL). Research is supported as part of the Solid-State Solar-Thermal Energy Conversion Center, an Energy Frontier Research Center funded by the U.S. Department of Energy, Office of Science, Basic Energy Sciences under Award No. DE-SC0001299/DE-FG02-09ER46577. Low-temperature magnetoresistance measurements made with support from Air Force Office of Scientific Research (AFOSR) Grants No. FA9550-15-1-0247 and No. FA9550-15-1-0377. The work at Argonne National Laboratory is supported by the U.S. Department of Energy, Office of Science, Basic Energy Sciences, Materials Sciences and Engineering Division under Contract No. DE-AC02-06CH11357. This work made use of the J. B. Cohen X-Ray Diffraction Facility supported by the Materials Research Science and Engineering Centers (MRSEC) program of the National Science Foundation (NSF) (Grant No. DMR-1121262) at the Materials Research Center of Northwestern University and the Soft and Hybrid Nanotechnology Experimental Resource (NSF Grant No. NNCI-1542205).

[1] D. M. Rowe, *CRC Handbook of Thermoelectrics* (CRC Press, Boca Raton, FL, 1995).

[2] C. B. Vining, W. Laskow, J. O. Hanson, R. R. Van der Beck, and P. D. Gorsuch, Thermoelectric properties of pressure-sintered $Si_{0.8}Ge_{0.2}$ thermoelectric alloys, J. Appl. Phys. **69**, 4333 (1991).

[3] S. R. Brown, S. M. Kauzlarich, F. Gascoin, and G. J. Snyder, $Yb_{14}MnSb_{11}$: New high efficiency thermoelectric material for power generation, Chem. Mater. **18**, 1873 (2006).

[4] S. Ohno, U. Aydemir, M. Amsler, J.-H. Pöhls, S. Chanakian, A. Zevalkink, M. A. White, S. K. Bux, C. Wolverton, and G. J. Snyder, Achieving $zT > 1$ in inexpensive Zintl phase $Ca_9Zn_{4+x}Sb_9$ by phase boundary mapping, Adv. Funct. Mater. **27**, 1606361 (2017).

[5] C. A. Uvarov, J. F. Rauscher, and S. M. Kauzlarich, High temperature thermoelectric properties of $Yb_{14-x}Ca_xMnSb_{11}$ made by reaction of the elements, Sci. Technol. Adv. Mater. **3**, 646 (2011).

[6] H. Jin, C. M. Jaworski, and J. P. Heremans, Enhancement in the figure of merit of *p*-type $Bi_{100-x}Sb_x$ alloys through multiple valence-band doping, Appl. Phys. Lett. **101**, 053904 (2012).

[7] S. Cho, A. DiVenere, G. K. Wong, J. B. Ketterson, and J. R. Meyer, Transport properties of $Bi_{1-x}Sb_x$ alloy thin films grown on CdTe(111)B, Phys. Rev. B **59**, 10691 (1999).

[8] D.-Y. Chung, T. P. Hogan, M. Rocci-Lane, P. Brazis, J. R. Ireland, C. R. Kannewurf, M. Bastea, C. Uher, and M. G. Kanatzidis, A new thermoelectric material: $CsBi_4Te_6$, J. Am. Chem. Soc. **126**, 6414 (2004).

[9] L. Lykke, B. B. Iversen, and G. K. H. Madsen, Electronic structure and transport in the low-temperature thermoelectric $CsBi_4Te_6$: Semiclassical transport equations, Phys. Rev. B **73**, 195121 (2006).

[10] D. A. Wright, Thermoelectric properties of bismuth telluride and its alloys, Nature (London) **181**, 834 (1958).

[11] D. Kusano and Y. Hori, Thermoelectric properties of *p*-type $(Bi_2Te_3)_{0.2}(Sb_2Te_3)_{0.8}$ thermoelectric material doped with PbTe, J. Jpn. Inst. Met. **66**, 1063 (2002).

[12] S. LeBlanc, Thermoelectric generators: Linking material properties and systems engineering for waste heat recovery applications, Sustain. Mater. Technol. **1**, 26 (2014).

[13] R. T. Littleton IV, T. M. Tritt, J. W. Kolis, and D. R. Ketchum, Transition-metal pentatellurides as potential low-temperature thermoelectric refrigeration materials, Phys. Rev. B **60**, 13453 (1999).

[14] N. D. Lowhorn, T. M. Tritt, E. E. Abbott, and J. W. Kolis, Enhancement of the power factor of the transition metal pentatelluride $HfTe_5$ by rare-earth doping, Appl. Phys. Lett. **88**, 022101 (2006).

[15] B. M. Zawilski, R. T. Littleton IV, and T. M. Tritt, Investigation of the thermal conductivity of the mixed pentatellurides $Hf_{1-x}Zr_xTe_5$, Appl. Phys. Lett. **77**, 2319 (2000).

[16] S. A. Miller, P. Gorai, B. R. Ortiz, A. Goyal, D. Gao, S. A. Barnett, T. O. Mason, G. J. Snyder, Q. Lv, V. Stevanović, and E. S. Toberer, Capturing anharmonicity in a lattice thermal conductivity model for high-throughput predictions, Chem. Mater. **29**, 2494 (2017).

[17] J. Yan, P. Gorai, B. Ortiz, S. Miller, S. A. Barnett, T. Mason, V. Stevanović, and E. S. Toberer, Material descriptors for predicting thermoelectric performance, Energy Environ. Sci. **8**, 983 (2015).

[18] P. Gorai, D. Gao, B. Ortiz, S. Miller, S. A. Barnett, T. Mason, Q. Lv, V. Stevanović, and E. S. Toberer, TE Design Lab: A virtual laboratory for thermoelectric material design, Comput. Mater. Sci. **112**, 368 (2016).

[19] P. Gorai, E. S. Toberer, and V. Stevanović, Computational identification of promising thermoelectric materials among known quasi-2D binary compounds, J. Mater. Chem. A **4**, 11110 (2016).

[20] E. F. Skelton, T. J. Wieting, S. A. Wolf, W. W. Fuller, D. U. Gubser, T. L. Francavilla, and F. Levy, Giant resistivity and x-ray diffraction anomalies in low-dimensional $ZrTe_5$ and $HfTe_5$, Solid State Commun. **42**, 1 (1982).

[21] F. J. DiSalvo, R. M. Fleming, and J. V. Waszczak, Possible phase transition in the quasi-one-dimensional materials $ZrTe_5$ or $HfTe_5$, Phys. Rev. B **24**, 2935 (1981).

[22] S. Okada, T. Sambongi, M. Ido, Y. Tazuke, R. Aoki, and O. Fujita, Negative evidences for charge/spin density wave in $ZrTe_5$, J. Phys. Soc. Jpn. **51**, 460 (1982).

[23] M. Rubinstein, $HfTe_5$ and $ZrTe_5$: Possible polaronic conductors, Phys. Rev. B **60**, 1627 (1999).

[24] P. Shahi, D. J. Singh, J. P. Sun, L. X. Zhao, G. F. Chen, J.-Q. Yan, D. G. Mandrus, and J.-G. Cheng, Bipolar conduction is the origin of the electronic transition in pentatellurides: Metallic vs. semiconducting behavior, arXiv:1611.06370.

[25] H. Chi, C. Zhang, G. Gu, D. E. Kharzeev, X. Dai, and Q. Li, Lifshitz transition mediated electronic transport anomaly in bulk $ZrTe_5$, New J. Phys. **19**, 015005 (2017).

[26] W. Yu, Y. Jiang, J. Yang, Z. L. Dun, H. D. Zhou, Z. Jiang, P. Lu, and W. Pan, Quantum oscillations at integer and fractional Landau level indices in single-crystalline $ZrTe_5$, Sci. Rep. **6**, 35357 (2016).

[27] H. Weng, X. Dai, and Z. Fang, Transition-Metal Pentatelluride $ZrTe_5$ and $HfTe_5$: A Paradigm for Large-Gap Quantum Spin Hall Insulators, Phys. Rev. X **4**, 011002 (2014).

[28] Q. Li, D. E. Kharzeev, C. Zhang, Y. Huang, I. Pletikosić, A. V. Fedorov, R. D. Zhong, J. A. Schneeloch, G. D. Gu, and T. Valla, Chiral magnetic effect in $ZrTe_5$, Nat. Phys. **12**, 550 (2016).

[29] H. Wang, C.-K. Li, H. Liu, J. Yan, J. Wang, J. Liu, Z. Lin, Y. Li, Y. Wang, L. Li, D. Mandrus, X. C. Xie, J. Feng, and J. Wang, Chiral anomaly and ultrahigh mobility in crystalline $HfTe_5$, Phys. Rev. B **93**, 165127 (2016).

[30] H. Wang, H. Liu, Y. Li, Y. Liu, J. Wang, J. Liu, Y. Wang, L. Li, J. Yan, D. Mandrus, X. C. Xie, and J. Wang, Discrete scale invariance and fermionic Efimov states in ultraquantum $ZrTe_5$, arXiv:1704.00995.

[31] Z. Fan, Q.-F. Liang, Y. B. Chen, S.-H. Yao, and J. Zhou, Transition between strong and weak topological insulator in $ZrTe_5$ and $HfTe_5$, Sci. Rep. **7**, 45667 (2017).

[32] D. N. McIlroy, S. Moore, D. Zhang, J. Wharton, B. Kempton, R. Littleton, M. Wilson, T. M. Tritt, and C. G. Olson, Observation of a semimetal-semiconductor phase transition in the intermetallic $ZrTe_5$, J. Phys. Condens. Matter **16**, L359 (2004).

[33] X.-B. Li, W.-K. Huang, Y.-Y. Lv, K.-W. Zhang, C.-L. Yang, B.-B. Zhang, Y. B. Chen, S.-H. Yao, J. Zhou, M.-H. Lu, L. Sheng, S.-C. Li, J.-F. Jia, Q.-K. Xue, Y.-F. Chen, and D.-Y. Xing, Experimental Observation of Topological Edge States at the Surface Step Edge of the Topological Insulator $ZrTe_5$, Phys. Rev. Lett. **116**, 176803 (2016).

[34] R. Wu, J.-Z. Ma, S.-M. Nie, L.-X. Zhao, X. Huang, J.-X. Yin, B.-B. Fu, P. Richard, G.-F. Chen, Z. Fang, X. Dai, H.-M. Weng, T. Qian, H. Ding, and S. H. Pan, Evidence for Topological Edge States in a Large Energy Gap Near the Step Edges on the Surface of $ZrTe_5$, Phys. Rev. X **6**, 021017 (2016).

[35] A. Pariari and P. Mandal, Coexistence of topological Dirac fermions on the surface and three-dimensional Dirac cone state in the bulk of $ZrTe_5$ single crystal, Sci. Rep. **7**, 40327 (2017).

[36] G. Zheng, J. Lu, X. Zhu, W. Ning, Y. Han, H. Zhang, J. Zhang, C. Xi, J. Yang, H. Du, K. Yang, Y. Zhang, and M. Tian, Transport evidence for the three-dimensional Dirac semimetal phase in $ZrTe_5$, Phys. Rev. B **93**, 115414 (2016).

[37] K. A. Borup, E. S. Toberer, L. D. Zoltan, G. Nakatsukasa, M. Errico, J.-P. Fleurial, B. B. Iversen, and G. J. Snyder, Measurement of the electrical resistivity and Hall coefficient at high temperatures, Rev. Sci. Instrum. **83**, 123902 (2012).

[38] C. Wood, D. Zoltan, and G. Stapfer, Measurement of Seebeck coefficient using a light pulse, Rev. Sci. Instrum. **56**, 719 (1985).

[39] A. F. May and G. J. Snyder, *Materials, Preparation, and Characterization in Thermoelectrics* (CRC Press, Boca Raton, FL, 2012), pp. 1–18.

[40] A. F. May, D. J. Singh, and G. J. Snyder, Influence oband structure on the large thermoelectric performance of lanthanum telluride, Phys. Rev. B **79**, 153101 (2009).

[41] D. J. Singh and W. E. Pickett, Skutterudite antimonides: Quasilinear bands and unusual transport, Phys. Rev. B **50**, 11235 (1994).

[42] D. J. Singh and I. I. Mazin, Calculated thermoelectric properties of La-filled skutterudites, Phys. Rev. B **56**, R1650 (1997).

[43] R. T. Littleton IV, T. M. Tritt, C. R. Feger, J. Kolis, M. L. Wilson, M. Marone, J. Payne, D. Verebeli, and F. Levy, Effect of Ti substitution on the thermoelectric properties of the pentatelluride materials $M_{1-x}Ti_xTe_5$ (M = Hf, Zr), Appl. Phys. Lett. **72**, 2056 (1998).

[44] M. Izumi, K. Uchinokura, E. Matsuura, and S. Harada, Hall effect and transverse magnetoresistance in a low-dimensional conductor $HfTe_5$, Solid State Commun. **42**, 773 (1982).

[45] M. Izumi, T. Nakayama, K. Uchinokura, S. Harada, R. Yoshizaki, and E. Matsuura, Shubnikov–de Haas oscillations and Fermi surfaces in transition-metal pentatellurides $ZrTe_5$ and $HfTe_5$, J. Phys. C **20**, 3691 (1987).

[46] W. W. Fuller, S. A. Wolf, T. J. Wieting, R. C. LaCoe, P. M. Chaikin, and C. Y. Huang, Pressure effects in $HfTe_5$ and $ZrTe_5$, J. Phys. (Paris), Colloq. **44**, C3-1709 (1983).

[47] R. T. Littleton IV, T. M. Tritt, J. W. Kolis, D. R. Ketchum, N. D. Lowhorn, and M. B. Korzenski, Suppression of the resistivity anomaly and corresponding thermopower behavior in the pentatelluride system by the addition of Sb: $Hf_{1-X}Zr_XTe_{5-Y}Sb_Y$, Phys. Rev. B **64**, 121104 (2001).

[48] T. E. Jones, W. W. Fuller, T. J. Wieting, and F. Levy, Thermoelectric power of $HfTe_5$ and $ZrTe_5$, Solid State Commun. **42**, 793 (1982).

[49] T. M. Tritt, N. D. Lowhorn, R. T. Littleton IV, A. Pope, C. R. Feger, and J. W. Kolis, Large enhancement of the resistive anomaly in the pentatelluride materials $HfTe_5$ and $ZrTe_5$ with applied magnetic field, Phys. Rev. B **60**, 7816 (1999).

[50] See the Supplemental Material at http://link.aps.org/supplemental/10.1103/PhysRevApplied.9.014025 for x-ray diffraction patterns, Rietveld refinement, and raw transport data.

[51] L. Akselrud and Y. Grin, WinCSD: Software package for crystallographic calculations (Version 4), J. Appl. Crystallogr. **47**, 803 (2014).

[52] H. Fjellvåg and A. Kjekshus, Structural properties of $ZrTe_5$ and $HfTe_5$ as seen by powder diffraction, Solid State Commun. **60**, 91 (1986).

[53] J. Wang, A. M. DaSilva, C.-Z. Chang, K. He, J. K. Jain, N. Samarth, X.-C. Ma, Q.-K. Xue, and M. H. W. Chan, Evidence for electron-electron interaction in topological insulator thin films, Phys. Rev. B **83**, 245438 (2011).

[54] Y. Zhang *et al.*, Electronic evidence of temperature-induced Lifshitz transition and topological nature in $ZrTe_5$, Nat. Commun. **8**, 15512 (2017).

[55] R. Y. Chen, S. J. Zhang, J. A. Schneeloch, C. Zhang, Q. Li, G. D. Gu, and N. L. Wang, Optical spectroscopy study of the three-dimensional Dirac semimetal $ZrTe_5$, Phys. Rev. B **92**, 075107 (2015).

[56] L. Moreschini, J. C. Johannsen, H. Berger, J. Denlinger, C. Jozwiak, E. Rotenberg, K. S. Kim, A. Bostwick, and M. Grioni, Nature and topology of the low-energy states in $ZrTe_5$, Phys. Rev. B **94**, 081101 (2016).

[57] R. Y. Chen, Z. G. Chen, X.-Y. Song, J. A. Schneeloch, G. D. Gu, F. Wang, and N. L. Wang, Magnetoinfrared Spectroscopy of Landau Levels and Zeeman Splitting of Three-Dimensional massless Dirac Fermions in $ZrTe_5$, Phys. Rev. Lett. **115**, 176404 (2015).

[58] Y. Liu, X. Yuan, C. Zhang, Z. Jin, A. Narayan, C. Luo, Z. Chen, L. Yang, J. Zou, X. Wu, S. Sanvito, Z. Xia, L. Li, Z. Wang, and F. Xiu, Zeeman splitting and dynamical mass generation in Dirac semimetal $ZrTe_5$, Nat. Commun. **7**, 12516 (2016).

[59] Y. Zhou, J. Wu, W. Ning, N. Li, Y. Du, X. Chen, R. Zhang, Z. Chi, X. Wang, X. Zhu, P. Lu, C. Ji, X. Wan, Z. Yang, J. Sun, W. Yang, M. Tian, Y. Zhang, and H.-k. Mao, Pressure-induced superconductivity in a three-dimensional topological material $ZrTe_5$, Proc. Natl. Acad. Sci. U.S.A. **113**, 2904 (2016).

[60] W. Shockley, *Electrons and Holes in Semiconductors* (Van Nostrand, Princeton, 1953).

[61] G. N. Kamm, D. J. Gillespie, A. C. Ehrlich, T. J. Wieting, and F. Levy, Fermi surface, effective masses, and Dingle temperatures of $ZrTe_5$ as derived from the Shubnikov–de Haas effect, Phys. Rev. B **31**, 7617 (1985).

[62] H. Xiong, J. A. Sobota, S.-L. Yang, H. Soifer, A. Gauthier, M.-H. Lu, Y.-Y. Lv, S.-H. Yao, D. Lu, M. Hashimoto, P. S. Kirchmann, Y.-F. Chen, and Z.-X. Shen, Three-dimensional nature of the band structure of $ZrTe_5$ measured by high-momentum-resolution photoemission spectroscopy, Phys. Rev. B **95**, 195119 (2017).

[63] G. Qiu, Y. Du, A. Charnas, H. Zhou, S. Jin, Z. Luo, D. Y. Zemlyanov, X. Xu, G. J. Cheng, and P. D. Ye, Observation of optical and electrical in-plane anisotropy in high-mobility few-layer $ZrTe_5$, Nano Lett. **16**, 7364 (2016).

[64] Y.-Y. Lv, F. Zhang, B.-B. Zhang, B. Pang, S.-H. Yao, Y. B. Chen, L. Ye, J. Zhou, S.-T. Zhang, and Y.-F. Chen, Microstructure, growth mechanism and anisotropic resistivity of quasi-one-dimensional $ZrTe_5$ crystal, J. Cryst. Growth **457**, 250 (2017).

[65] M. K. Hooda and C. S. Yadav, Enhanced thermopower and low thermal conductivity in *p*-type polycrystalline $ZrTe_5$, Appl. Phys. Lett. **111**, 053902 (2017).

[66] M.-H. Whangbo, F. J. DiSalvo, and R. M. Fleming, Electronic structure of $ZrTe_5$, Phys. Rev. B **26**, 687 (1982).

[67] N. D. Lowhorn, T. M. Tritt, E. E. Abbott, and J. W. Kolis, in *Proceedings of the 24th International Conference on Thermoelectrics, ICT 2005* (IEEE, New York, 2005), pp. 41–45.

[68] R. T. Littleton IV, Ph.D. thesis, Clemson University, 2001.